CO Adsorption on Fe4C (100), (110), and (111) Surfaces in Fischer–Tropsch Synthesis

ARTICLE *in* THE JOURNAL OF PHYSICAL CHEMISTRY C · NOVEMBER 2008

Impact Factor: 4.77 · DOI: 10.1021/jp805702n

7 AUTHORS, INCLUDING:

Chun-Fang Huo
Chinese Academy of Sciences
47 PUBLICATIONS **726** CITATIONS
SEE PROFILE

Gang Feng
Nanchang University
34 PUBLICATIONS **242** CITATIONS
SEE PROFILE

Yong-Wang Li
Chinese Academy of Sciences
406 PUBLICATIONS **7,336** CITATIONS
SEE PROFILE

Jianguo Wang
Northwestern Polytechnical University
209 PUBLICATIONS **3,284** CITATIONS
SEE PROFILE

CO Adsorption on Fe_4C (100), (110), and (111) Surfaces in Fischer−Tropsch Synthesis

Chun-Mei Deng,[†] Chun-Fang Huo,[†] Li-Li Bao,[†] Gang Feng,[†] Yong-Wang Li,[†] Jianguo Wang,[†] and Haijun Jiao*[,†,‡]

State Key Laboratory of Coal Conversion, Institute of Coal Chemistry, Chinese Academy of Sciences, Taiyuan, Shanxi 030001, P.R. China, Leibniz-Institut für Katalyse e.V. an der Universität Rostock, Albert-Einstein-Strasse 29a, 18059 Rostock, Germany

Received: June 29, 2008; Revised Manuscript Received: October 6, 2008

The adsorption of CO at various coverage on the termination surfaces of the low-indexed (100), (110), and (111) surfaces of Fe_4C has been performed at the level of density functional theory. It is found that CO prefers to adsorb around Fe atoms. It is also found that there is no significant lateral interaction between the adsorbed CO at 1/4 monolayer (ML) coverage, whereas there is stronger repulsive interaction at 1 ML for (100) and (110) surfaces, and 1/2 ML for (111) surface. It is also interesting to note that the surface ketenylidene (C═C═O) species on (100) $T_{Fe/C}$, (110) $T_{Fe/C}$, and (111) T_C may be the precursor for CO dissociation. On all surfaces, the adsorbed CO is partially negatively charged, indicating the enhanced electron transfer from the Fe_4C surface to CO, and the more the electron transfer, the stronger the CO activation.

1. Introduction

CO adsorption on the low-indexed surfaces of transition metals has been the subject of numerous experimental and theoretical studies because of its crucial role in many catalytic processes; for example, in car exhaust or Fischer−Tropsch synthesis (FTS). Both experimental and theoretical studies have indicated CO adsorption to be likely dissociative on the left side of the first-row transition metals up to iron, but molecular on the right side from cobalt.[1−6] Sung and Hoffman[6] theoretically analyzed CO adsorption on transition metal surfaces and emphasized the synergetic donation and back-donation interaction between CO and metal as the most important interaction.

During the past 70 years, FTS has enjoyed great attention as an option for the production of clean transportation fuels and chemicals. Despite extensive experimental[7−10] and theoretical[11−15] studies, the reaction mechanisms of FTS remain uncertain because of the complexity of the coexisting phases and the difficulty in getting the microscopic information under real experimental conditions.

In FTS, iron-based catalysts are exposed to syngas ($CO + H_2$) and have complicated interchanges of different phases. Activation with carbon monoxide or syngas typically results in the conversion of Fe_2O_3 to Fe_3O_4 and, ultimately, to one or more iron carbides.[16] Several Fe phases, including α-Fe,[17] Fe_3O_4,[18,19] Fe_4C,[20] θ-Fe_3C,[21] χ-Fe_5C_2[22], Fe_7C_3[23], and ε'-$Fe_{2.2}C$,[24] were detected in freshly activated or used Fe-based FTS catalysts. It is generally believed that iron carbides are FTS active phases, whereas Fe_3O_4 is the active phase for a water−gas shift reaction. The phase formation and transformation of iron carbides in fused catalysts change with temperature. For example, Fe_2C and $Fe_{2.2}C$ phases are formed simultaneously at low temperatures (115 °C), but only Fe_2C phase at 150−185 °C; in the range 220−400 °C, Fe_5C_2 phase is formed; and the final stable Fe_3C phase is formed at 450 °C.[25]

For deeper insights into the detailed mechanisms, it is desired and necessary to study CO adsorption on each type of the active phases due to the key role of CO adsorption in the FTS. In our previous work, the adsorption of CO on α-Fe,[26−28] Fe_3O_4,[29] Fe_3C,[30] and Fe_5C_2[31,32] was investigated. On Fe(111), the shallow-hollow adsorption of CO is the most stable site at 1/3 and 1/2 monolayer (ML), whereas both shallow-hollow and bridge adsorption can coexist at 1 ML.[26] On the Fe_{oct2}- and Fe_{tet1}-terminated Fe_3O_4(111) surfaces, the on-top adsorption modes are most stable.[29] Studies of CO adsorption on carbides showed that CO prefers to interact with Fe atoms on carbide surfaces. On Fe_3C, CO favors the three-fold site of (100) and the four-fold site of (001), but the two-fold site and three-fold site of (010) at low coverage.[30] On Fe_5C_2, CO prefers to adsorb on the three-fold iron site of (001), (110), and (100).[31]

There are two types of Fe_4C: (i) with octahedral interstitial carbon atoms (Fe_4C/oct), and (ii) with tetrahedral interstitial carbons (Fe_4C/tet).[33,34] In our previous work,[35] we have studied the structure and stability of Fe_4C bulk and surfaces and found that Fe_4C/oct is more stable than Fe_4C/tet, and the termination with surface carbon atoms tends to be more stable for the same crystallographic orientation. The electronic structure and magnetic properties of Fe_4C were studied by Santos et al.[36] It was observed that the behavior of the magnetic moments, hyperfine field, and isomer shift with volume shows some similarities to the related compound Fe_4N.

In this work, we used spin-polarized density functional theory (DFT) to study the interaction of CO with the low-indexed (100), (110), and (111) surfaces of Fe_4C for exploring the FTS mechanism. The site preference of CO on the surfaces and the partial density of states (PDOS) for the adsorbed species were examined.

2. Methods and Models

(a) Method. We performed first-principle calculation based on spin-polarized DFT.[37,38] All calculations were carried out by using the Cambridge sequential total energy package.[39−41] The exchange and correlation energies were calculated using the Perdew, Burke,and Ernzerhof functional[42] within the generalized gradient approximation (GGA-PBE).[43] Ionic cores were described by the ultrasoft pseudopotential,[44] and the Kohn−Sham

* Corresponding author. E-mail: haijun.jiao@catalysis.de.
† Chinese Academy of Sciences.
‡ Leibniz-Institut für Katalyse e.V. an der Universität Rostock.

10.1021/jp805702n CCC: $40.75
Published on Web 11/07/2008

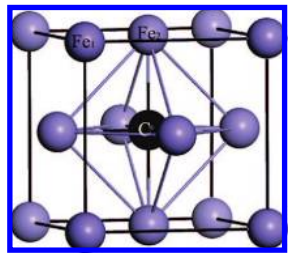

Figure 1. Schematic view of the Fe_4C unit cell with octahedral interstitial carbon.

one-electron states were expanded in a plane wave basis set up to 340 eV. A Fermi smearing of 0.1 eV was utilized. Brillouin zone integration was approximated by a sum over special *k*-points chosen using the Monkhorst−Pack scheme.[45] Because of its large effect on magnetic systems, spin polarization was included in the calculation of Fe_4C to correctly account for its magnetic properties. Without counting the adsorbates, the vacuum between the slabs was set to span a range of 10 Å to exclude interactions between the periodic slabs. The convergence criteria for structure optimization and energy calculation were set to medium quality with the tolerance for SCF, energy, maximum force, and maximum displacement of 2.0×10^{-6} eV/atom, 2.0×10^{-5} eV/atom, 0.05 eV/Å and 2.0×10^{-3} Å, respectively.

It should be noted that the PBE functional can give reasonable optimized geometries but tends to overestimate the adsorption energies. We therefore present results of the revised exchange and correlation functional (GGA-RPBE). RPBE appears to give a better description of atomization energies of molecules and adsorption energies.[46,47] Therefore, we used PBE for geometry optimizations and further carried out RPBE single-point energy calculations on the relaxed PBE structures. We used the RPBE energies for discussion and the PBE values for comparison.

(b) Model. On the basis of our previous work, the more stable Fe_4C with octahedral interstitial carbon atoms (Fe_4C/oct) was chosen for studying CO adsorption. As shown in Figure 1, Fe_4C/oct has two nonequivalent Fe sites; that is, the corner site (Fe_1) without nearest neighbor C atoms and the face-centered site (Fe_2) with two C atoms in the first interstitial shell. Using a *k*-point mesh of $6 \times 6 \times 6$, the optimized equilibrium constant for bulk Fe_4C/oct is 3.740 Å. The magnetic moments are found to be 3.12 μ_B for Fe_1 and 1.74 μ_B for Fe_2. These values agree well with previous theoretical values of 3.765 Å, 2.98 μ_B, and 1.75 μ_B, respectively.[48] This indicates the methods used in our calculations are reliable and reasonable.

Fe_4C/oct has three low-indexed (100), (110) and (111) surfaces and each surface has two terminations, as shown in Figure 2. Both (100) and (110) have iron (T_{Fe}) as well as mixed iron and carbon ($T_{Fe/C}$) terminations, and (111) has pure iron (T_{Fe}) and pure carbon (T_C) terminations. Because of their close surface energies[35] and different surface structure, it is worth to study CO adsorption on all surface terminations. Figure 2 displays the potential surface adsorption sites, which are signed by using the alphabets (from a to u). The detailed illustrations are given in the next section.

The adsorption energy per CO molecule (E_{ads}) is defined as: $E_{ads} = [E_{CO/slab} - (nE_{CO} + E_{slab})]/n$; where $E_{CO/slab}$, E_{CO}, and E_{slab} are the total energies for the slabs with adsorbed CO on the surface, the isolated CO molecule, and the slab of the clean surface, respectively, and n is the number of adsorbed CO molecules. Therefore, the more negative the E_{ads}, the stronger the adsorption. The coverage (θ) is defined as the number of CO molecules over the number of the first-layer iron atoms. The Mulliken atomic charges were used for discussing the effects of charge transfer.

To discuss CO coverage effect, slab models with different sizes are used. For (100), a p($\sqrt{2} \times \sqrt{2}$) unit cell with $4 \times 4 \times 1$ *k*-mesh was used for 1/4 ML by putting one CO molecule, while a p(1×1) unit cell with $5 \times 5 \times 1$ *k*-mesh was used for 1/2 and 1 ML by putting one and two CO molecules, respectively. For (110), a p(2×1) unit cell with $3 \times 4 \times 1$ *k*-mesh was used for 1/4 ML by putting one CO molecule, while a p(1×1) unit cell with $5 \times 4 \times 1$ *k*-mesh for 1/2 and 1 ML by putting one and two CO molecules, respectively. In addition, a p(1×1) unit cell with $4 \times 4 \times 2$ *k*-mesh was used for 1/4 and 1/2 ML by putting one and two CO molecules, respectively, on the (111) surface.

First, four-layer models were used and further validated by models with five and six layers. For four-layer models, the top two layers were allowed to relax while the two bottom layers were fixed in their bulk positions. For five- and six-layer models, both the top two and three layers were allowed to relax, respectively, and the corresponding bottom layers were fixed in their bulk positions. As given in Table 1, benchmark calculations on the most stable adsorption structures (**17**, **32**, and **59**) show that the maximal change of the adsorption energies is less than 0.05 eV (<2.7%), and the maximal change of the C−O bond lengths is up to 0.007 Å. Therefore, the four-layer slab models with relaxation of the top two layers are reasonable.

3. Results and Discussion

(a) CO Adsorption on (100) T_{Fe}. At 1/4 ML CO coverage, five types of adsorption sites were considered (Figure 2a, b, d, h, r), and only three stable configurations (**1**−**3**) were found (Figure 3). The calculated adsorption energies, structural parameters, and net charges are given in Table 2. **1** (T-b) and **2** (3F-h) have CO adsorption at the Fe_2-top site and the 3-fold site (Fe_1-2Fe_2), respectively. In **3** (4F-r), CO adsorbs at the 4-fold site ($2Fe_1-2Fe_2$), with the O atom bonding to two Fe (Fe_1-Fe_2) atoms, and CO is highly activated, as indicated by the elongated C−O distance of 1.288 Å. The adsorption energies of **1**−**3** are −1.95, −1.78, and −1.98 eV, respectively, and **1** and **3** are more stable adsorption structures.

At high coverage of 1/2 ML, CO adsorption yields four stable configurations (**4**−**7**, Figure 3). The structures of **5** (T-b) and **7** (4F-r) are similar to those of **1** and **3** at 1/4 ML, respectively, whereas the adsorption energies (**5**, −1.79 eV; and **7**, −1.89 eV) become lower. In **4** (T-a) and **6** (B-d), CO adsorb on the Fe_1-top site and bridge site (Fe_1-Fe_2) with adsorption energies of −1.58 and −1.12 eV, respectively. Configuration **7** is the most stable and also with the longest C−O distance (1.282 Å).

By increasing coverage to 1 ML (Table 2), the adsorption energy decreases, and this is mainly due to the increased repulsive interactions of the adsorbed CO molecules. Four stable adsorption configurations (**8**−**11**) are located. In the most stable configuration, **8** (B-d/B-d), both CO molecules adsorb at the bridge site (Fe_1-Fe_2), and the adsorption energy is −1.05 eV. In **9**−**11**, one CO adsorbs at the 4-fold site (4F-r) and the other one, at the Fe_2-top, Fe_1-top, and bridge (Fe_1-Fe_2) site, respectively, and they have very close adsorption energies (−0.78, −0.77, and −0.79 eV, respectively).

(b) CO Adsorption on (100) $T_{Fe/C}$. At 1/4 ML, four stable configurations were obtained (**12**−**15**, Figure 4), and the computed adsorption energies, structural parameters, and net charges are listed in Table 3. Comparing the adsorption energies, CO prefers to adsorb around iron atoms. **15** (4F-s) with CO at

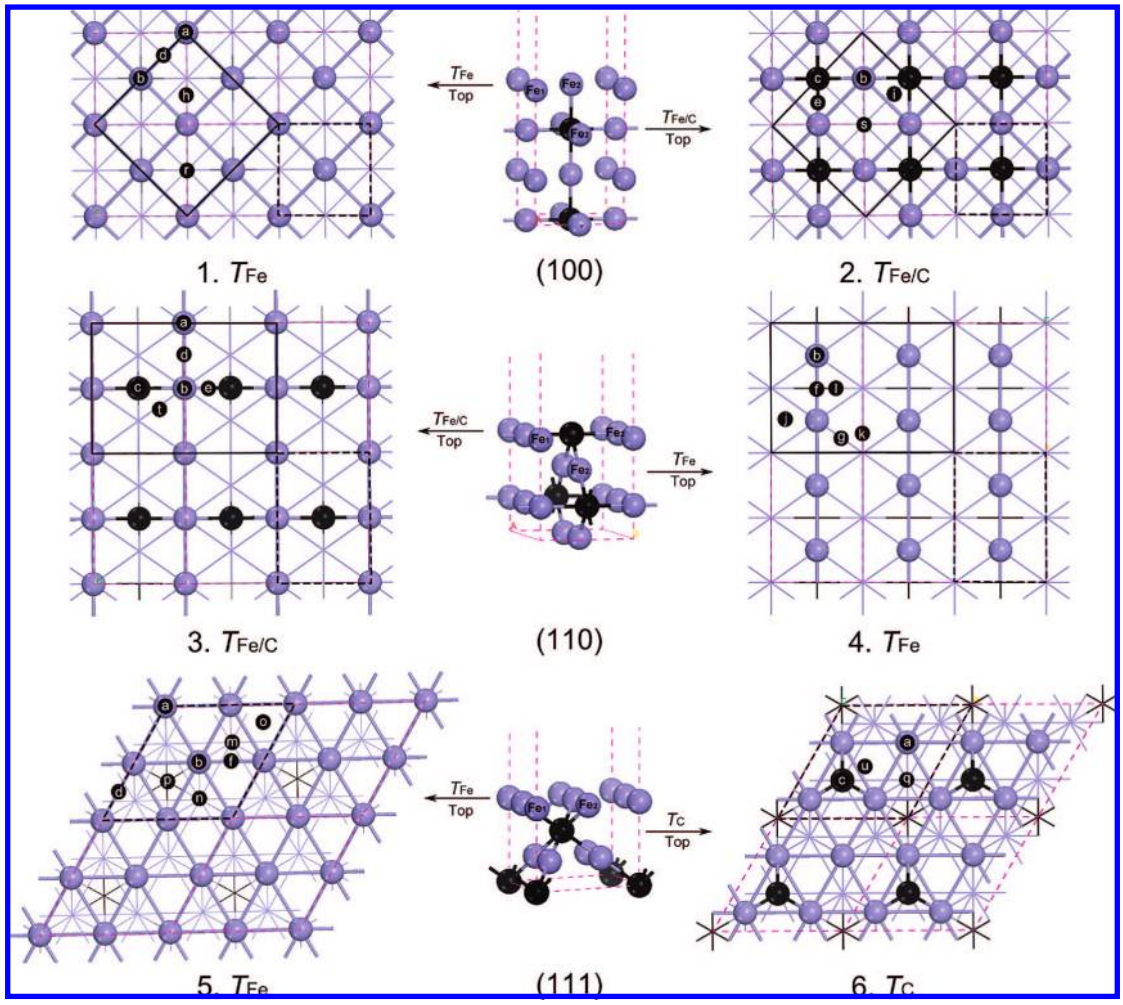

Figure 2. Top and side views of low-indexed Fe_4C surfaces: (1) solid frame in **1** and **2** for p($\sqrt{2} \times \sqrt{2}$), and in **3** and **4** for p(2 × 1); dashed frame in **1**, **2**, **3**, **4**, **5**, and **6** for p(1 × 1); and (2) on-top site (a−c), bridge site (d−g), 3-fold site (h−q), and 4-fold site (r−u).

TABLE 1: Thickness Influence on Adsorption Energy (E_{ads}, eV) and C−O Bond Length (d, Å)

surface	m/n[a]	E_{ads}	d_{C-O}	d_{C-Fe}
(100)/**17**	2/2	−1.40	1.161	1.753
	2/3	−1.41	1.161	1.755
	3/2	−1.41	1.161	1.754
	2/4	−1.44	1.161	1.752
	3/3	−1.45	1.162	1.749
(110)/**32**	2/2	−1.83	1.162	1.748
	2/3	−1.88	1.165	1.748
	3/2	−1.87	1.164	1.747
	2/4	−1.85	1.164	1.748
	3/3	−1.85	1.164	1.749
(111)/**59**	2/2	−2.54	1.182	2.293, 2.265, 1.793
	2/3	−2.58	1.189	2.156, 2.154, 1.821
	3/2	−2.58	1.189	2.147, 2.148, 1.826
	2/4	−2.57	1.187	2.191, 2.202, 1.809
	3/3	−2.59	1.188	2.178, 2.185, 1.816

[a] Number of the relaxed (m) and fixed (n) layers.

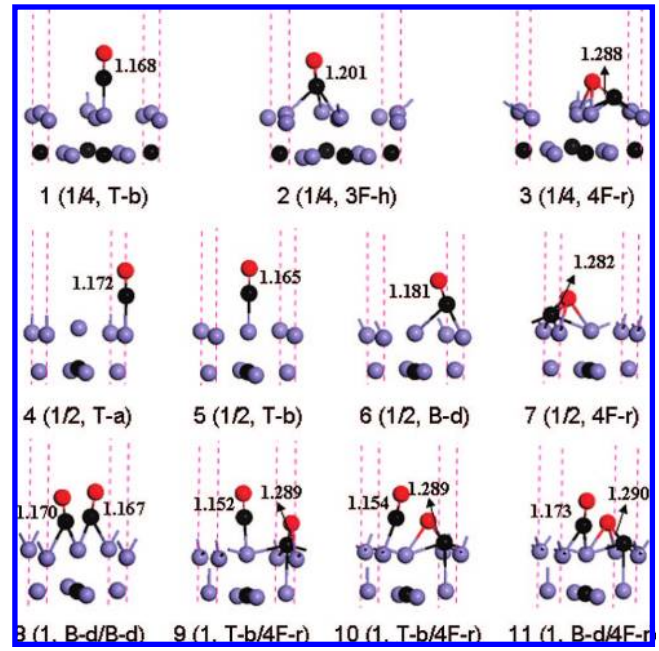

Figure 3. Side view of CO adsorption on (100) T_{Fe} (Fe, purple; C, black; O, red).

the 4-fold site ($4Fe_2$) and **13** (T-b) with CO at the Fe_2-top site have close adsorption energies (−1.10 and −1.04 eV, respectively). However, **12** (T-c) with CO at the C-top site, and **14** (B-e) with CO bridging over Fe_2 and C atoms are not competitive (−0.67 and −0.61 eV, respectively). In **12**−**15**, the C−O bond lengths are from 1.162 to 1.211 Å, longer than that (1.145 Å) of free CO.

At 1/2 ML, there are also four stable adsorption configurations (**16**−**19**, Figure 4). As given in Table 3, the structures at 1/2 ML are close to those at 1/4 ML, whereas the adsorption energies decrease, except for **17** (T-b). At 1/2 ML, **17** with CO

TABLE 2: Calculated Adsorption Energies (E_{ads}, eV) per CO and Bond Lengths (d, Å) As Well As Net Charges (q) of CO on (100) T_{Fe} at 1/4, 1/2, and 1 ML

no.	θ	E_{ads}[a]	d_{C-O}	d_{Fe-C}	d_{O-Fe}	q_{CO}
1	1/4	−1.95 (−2.24)	1.168	1.792		−0.28
2	1/4	−1.78 (−2.18)	1.201	1.938, 2.061, 2.062		−0.57
3	1/4	−1.98 (−2.53)	1.288	1.999, 2.205, 2.139, 1.897	2.228, 2.030	−0.80
4	1/2	−1.58 (−1.88)	1.172	1.781		−0.28
5	1/2	−1.79 (−2.06)	1.165	1.801		−0.23
6	1/2	−1.12 (−1.14)	1.181	1.765, 2.236		−0.35
7	1/2	−1.89 (−2.45)	1.282	2.091, 1.960, 2.091, 1.902	2.191, 2.064	−0.79
8	1	−1.05 (−1.50)	1.170	2.190, 1.783		−0.29
			1.167	2.283, 1.766		−0.27
9	1	−0.78 (−1.26)	1.152	1.837		−0.09
			1.289	1.931, 2.057, 1.978, 1.980	1.999	−0.78
10	1	−0.77 (−1.26)	1.154	1.806		−0.10
			1.289	1.972, 1.981, 1.947, 1.981	1.953	−0.81
11	1	−0.79 (−1.32)	1.173	1.869, 1.975		−0.28
			1.290	1.927, 1.948, 1.934, 1.945	2.071, 2.042	−0.79

[a] PBE values in parentheses.

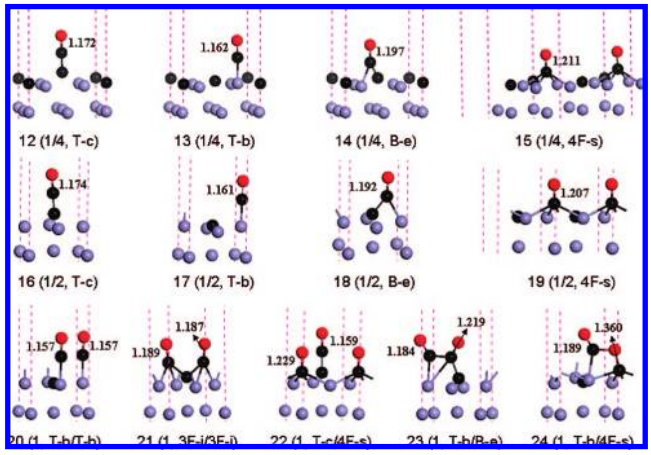

Figure 4. Side view of CO adsorption on (100) $T_{Fe/C}$ (Fe, purple; C, black; O, red).

at the Fe_2-top site becomes the most stable (−1.08 eV), followed by **19** (4F-s) with CO at the 4-fold site (−0.93 eV). Similarly, the C-top (**16**, (T-c)) and Fe−C bridge (**18** (B-e)) modes are not competitive. In addition, the most activated C−O bond is found in **19** (4F-s) (1.207 Å).

At 1 ML (**20**−**24**), the adsorption energy further decreases: **21** (3F-i/3F-i), **23** (T-b/B-e) and **24** (T-b/4F-s) even have positive adsorption energies (0.11, 0.52, and 0.33 eV, respectively), indicating that CO adsorption at high coverage on (100) is thermodynamically not favored. In the stable configurations (**20** (T-b/T-b) and **22** (T-c/4F-s), CO tends to occupy the top site to minimize the repulsive interactions.

(c) CO Adsorption on (110) $T_{Fe/C}$. Table 4 lists the computed adsorption energies and the structure parameters for the stable adsorbed CO on (110) $T_{Fe/C}$; the structures of adsorption configurations are shown in Figure 5. At 1/4 ML, six stable configurations (**25**−**30**) were found. In **25** (T-a) and **26** (T-b), CO binds with one iron atom (Fe_1 and Fe_2, respectively) but with one C atom in **27** (T-c). Configuration **26** is the most stable (−1.52 eV), and **25** is the least stable (−0.98 eV). In **28** (B-d) and **29** (B-e), CO adsorbs at a 2-fold site. Configuration **28** with CO bridging over two iron atoms is more stable than **29** with CO bridging over Fe_2 and C atoms on the basis of the adsorption energies (−1.46 and −1.40 eV, respectively). In **30** (4F-t), CO adsorbs at a 4-fold site (Fe_1−Fe−-Fe_2'−C). Interestingly, the O atom of **30** interacts with the Fe_1 atom, forming surface ketenylidene (C═C═O). The activated C−O bond is 1.216 Å, much longer than those in **25**−**29**.

At 1/2 ML, five stable configurations (**31**−**35**) were obtained. As given in Table 4, the adsorption energies decrease with an increase in CO coverage, except for **32** (T-b) and **35** (4F-t). Configuration **32** with CO at the Fe_2-top site is the most stable (−1.57 eV), followed by **35** (4F-t), **34** (B-e), and **33** (T-c) (−1.45, −1.30, and −1.26 eV, respectively), whereas **31** (T-a) with CO at the Fe_1-top site is the least stable (−0.96 eV).

At 1 ML, putting two CO molecules in one p(1 × 1) unit cell yields seven stable configurations (**36**−**42**, Figure 5). It is noteworthy that the CO adsorbed sites can be considered as combinations of the occupied sites in **25**−**30**. For example, **36** (T-a/T-c) has the same adsorbed sites as **25** and **27**, and **37** (B-e/4F-t) has the same adsorbed sites as **29** and **30**. As given in Table 4, the most stable structures (**38** (B-d/T-b) and **41** (B-d/B-e)) have adsorption energies of only −1.20 and −1.19 eV, respectively, lower than those of **26**, **28**, and **29**.

(d) CO Adsorption on (110) T_{Fe}. The pure iron termination surface of (110) is steplike with atoms of the first and second layers exposed. Since the carbon atoms in the second layer are buried under iron atoms in the first layer, CO could adsorb on only the Fe atoms in the first and second layers. The optimized structures of CO adsorption at 1/4, 1/2, and 1 ML are displayed in Figure 6, and the corresponding bond parameters and adsorption energies are given in Table 5. As shown in Figure 6, there are four stable adsorption configurations (**43**−**46**) at 1/4 ML. Configuration **43** (T-b) and **44** (B-f) have CO adsorption on the Fe_2-top and Fe_2−Fe_2 bridge site, respectively. In **45** (3F-l) and **46** (3F-l), CO adsorbs at the 3-fold site ($2Fe_2$−Fe_1), and the tilted adsorption geometry is found in **46** with the O atom bonding to two Fe_2 atoms. Configuration **46** is also the most stable adsorption configuration with the highest adsorption energy (−2.22 eV).

At 1/2 ML, five stable adsorption configurations were found (**47**−**51**). The structures of **47** (T-b), **48** (B-f), and **49** (3F-l) are similar to **43**, **44**, and **45**, respectively, whereas the adsorption energies decrease (−1.09 vs −1.21; −1.93 vs −2.04; −1.52 vs −1.61 eV, respectively). Configuration **48** is the most stable adsorption structure. In **50** (3F-j) and **51**(3F-j), the C−O axis of the adsorbed CO is tilted with the O atom bonding to the Fe_2 atom, and the activated C−O bond is 1.315 and 1.258 Å, respectively, much longer than those in **47**−**49**.

At 1 ML, five stable adsorption configurations (**52**−**56**) were located. Configuration **53** (T-b/3F-l) is the most stable (−1.59 eV), with one CO adsorbing on the Fe_2-top site and one at the 3-fold site.

TABLE 3: Calculated Adsorption Energies (E_{ads}, eV) per CO and Bond Lengths (d, Å) As Well As Net Charges (q, e) of CO on (100) $T_{Fe/C}$ at 1/4, 1/2, and 1 ML

no.	θ	E_{ads}[a]	d_{C-O}	d_{Fe-C}	d_{C-C}	q_{CO}
12	1/4	−0.67 (−0.86)	1.172		1.323	−0.03
13	1/4	−1.04 (−1.36)	1.162	1.758		−0.15
14	1/4	−0.61 (−0.97)	1.197	1.876	1.449	−0.31
15	1/4	−1.10 (−1.54)	1.211	2.052, 2.056, 2.055, 2.051		−0.57
16	1/2	−0.50 (−0.74)	1.174		1.318	−0.07
17	1/2	−1.08 (−1.40)	1.161	1.753		−0.15
18	1/2	−0.59 (−0.94)	1.192	1.889	1.452	−0.26
19	1/2	−0.93 (−1.34)	1.207	2.083, 2.084, 2.093, 2.094		−0.53
20	1	−0.84 (−0.84)	1.157	1.752		−0.12
			1.157	1.752		−0.12
21	1	0.11 (−0.41)	1.189	1.914, 2.181	1.470	−0.23
			1.187	1.901, 2.012	1.614	−0.27
22	1	−0.51 (−0.66)	1.159		1.345	0.12
			1.229	2.047, 2.044, 2.068, 2.065		−0.62
23	1	0.52 (−0.15)	1.219	2.331	1.452	−0.22
			1.184	1.990	1.478	−0.12
24	1	0.33 (−0.29)	1.189	1.969		−0.02
			1.360 1.397	2.140, 2.060, 1.997, 1.887		−0.60

[a] PBE values in parentheses.

TABLE 4: Calculated Adsorption Energies (E_{ads}, eV) per CO and Bond Lengths (d, Å) As Well As Net Charges (e) of CO on (110) $T_{Fe/C}$ at 1/4, 1/2, and 1 ML

no.	θ	E_{ads}[a]	d_{C-O}	d_{Fe-C}	d_{C-C}	d_{Fe-O}	q_{CO}
25	1/4	−0.98 (−1.27)	1.167	1.778			−0.24
26	1/4	−1.52 (−1.81)	1.166	1.738			−0.21
27	1/4	−1.37 (−1.61)	1.180		1.316		−0.13
28	1/4	−1.46 (−1.76)	1.173	2.326,1.773			−0.30
29	1/4	−1.40 (−1.68)	1.195	2.007	1.365		−0.28
30	1/4	−1.45 (−1.84)	1.216	2.123,1.890,2.343	1.391	2.105	−0.59
31	1/2	−0.96 (−1.22)	1.162	1.818			−0.20
32	1/2	−1.57 (−1.84)	1.166	1.741			−0.20
33	1/2	−1.26 (−1.49)	1.179		1.319		−0.12
34	1/2	−1.30 (−1.57)	1.191	2.015	1.367		−0.24
35	1/2	−1.45 (−1.85)	1.259	2.109,1.894,2.381	1.385	2.077	−0.56
36	1	−1.04 (−1.24)	1.168	1.768			−0.24
			1.169		1.327		−0.02
37	1	−1.05 (−1.44)	1.193	1.892	1.458		−0.25
			1.256	2.059,1.885,2.191	1.419	2.060	−0.55
38	1	−1.20 (−1.54)	1.159	1.757			−0.16
			1.184	1.962, 1.881			−0.38
39	1	−0.78 (−1.15)	1.221	2.300	1.452		−0.22
			1.242	2.175,1.902	1.493	2.004	−0.31
40	1	−1.14 (−1.51)	1.160	1.761			−0.16
			1.253	2.037,1.926,2.263	1.391	2.162	−0.57
41	1	−1.19 (−1.54)	1.196	1.940	1.408		−0.27
			1.175	2.111, 1.794			−0.33
42	1	−1.09 (−1.46)	1.171	2.061, 1.882			−0.29
			1.167	2.180, 1.840			−0.26

[a] PBE values in parentheses.

(e) CO Adsorption on (111) T_{Fe}. The termination surface layer of (111) has only surface Fe atoms. As shown in Figure 7, there are three 3-fold (**58**−**60**) and one top (**57**) models for CO adsorption at 1/4 ML, and the calculated adsorption energies and structure parameters are listed in Table 6. Configuration **57** (T-a) with CO at the Fe_1-top site and **60** (3F-n) with CO at the 3-fold site (Fe_1-$2Fe_2$) have very close adsorption energies of −1.62 and −1.65 eV, while another 3-fold site ($3Fe_2$) (**58** (3F-p)) is the least stable (−1.34 eV), and **59** (3F-m) with CO at the 3-fold site ($3Fe_2$) is the most stable (−2.16 eV).

There are nine stable adsorption configurations (**61**−**69**) at 1/2 ML. In this case, the CO adsorbed sites can be considered as the combinations of the occupied sites in **57**−**60**. For example, **62** (T-a/3F-p) has the same adsorbed CO sites as **57** and **58**, and **63** (T-a/3F-m) has the same adsorbed CO sites as **57** and **59**. As given in Table 6, **64** (3F-n/3F-o) is the most stable (−1.81 eV), and **62** is the least stable (−1.20 eV). The adsorption energies of **65**−**68** with one CO at the top site are very close (−1.70 to −1.71 eV).

(f) CO Adsorption on (111) T_C. The pure carbon termination surface of (111) is very open, with Fe atoms of the second layer exposed; therefore, CO could bond to not only the surface C atoms but also the Fe atoms of the second layer. Both 1/4 and 1/2 ML are used to study CO adsorption on (111) T_C. Four stable adsorption configurations are found for each (**70**−**73** for 1/4 ML, **74**−**77** for 1/2 ML), as shown in Figure 8. In **72** (4F-u), CO adsorbs at the 4-fold site (Fe_1'−$2Fe_2'$−1C), with the O atom bonding with the Fe_1 atom, forming a C═C═O structure, and the C−O bond (1.243 Å) is the most activated. In **71** (T-a) and **73** (3F-q), CO adsorbs at the Fe_1-top and 3-fold sites (Fe_1'-$2Fe_2'$), respectively. It is notable that the surface C atoms in **73** move far away form the adsorbed CO (d_{C-C}: 3.149 vs 2.627 Å), indicating strong repulsive interaction between CO and the

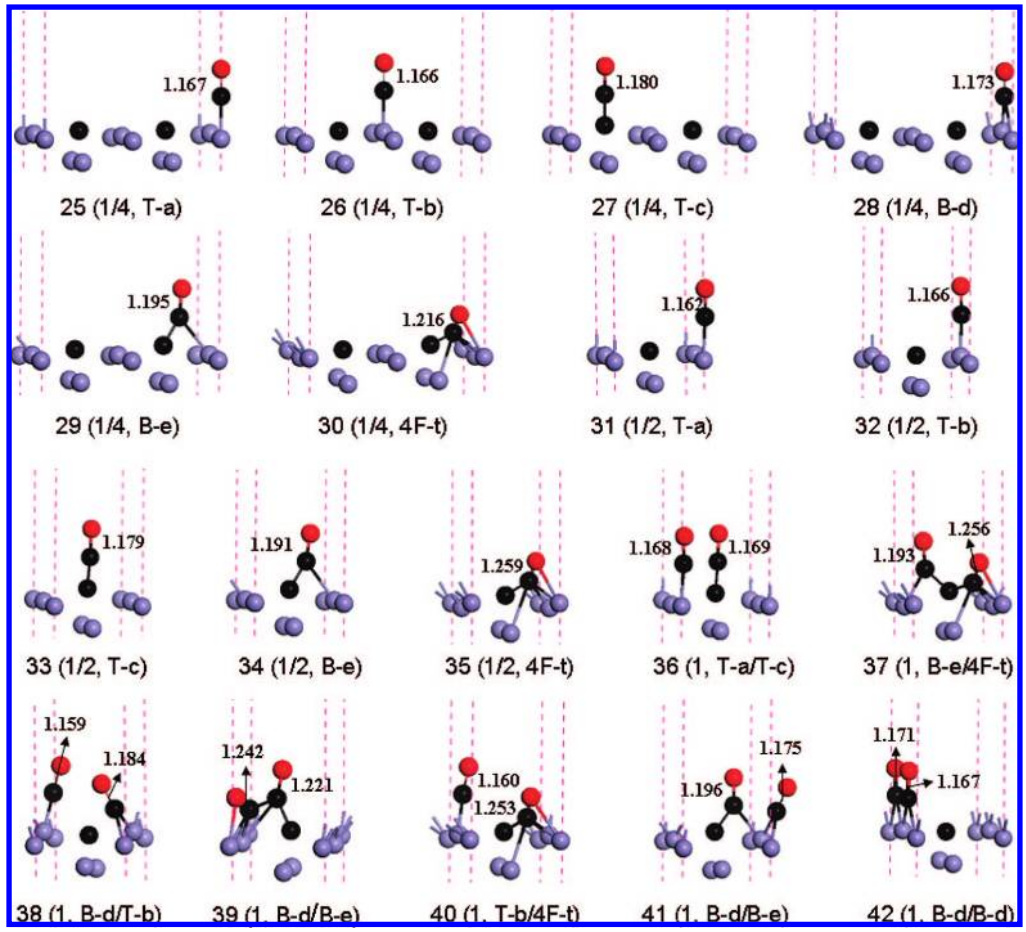

Figure 5. Side view of CO adsorption on (110) $T_{Fe/C}$ (Fe, purple; C, black; O, red).

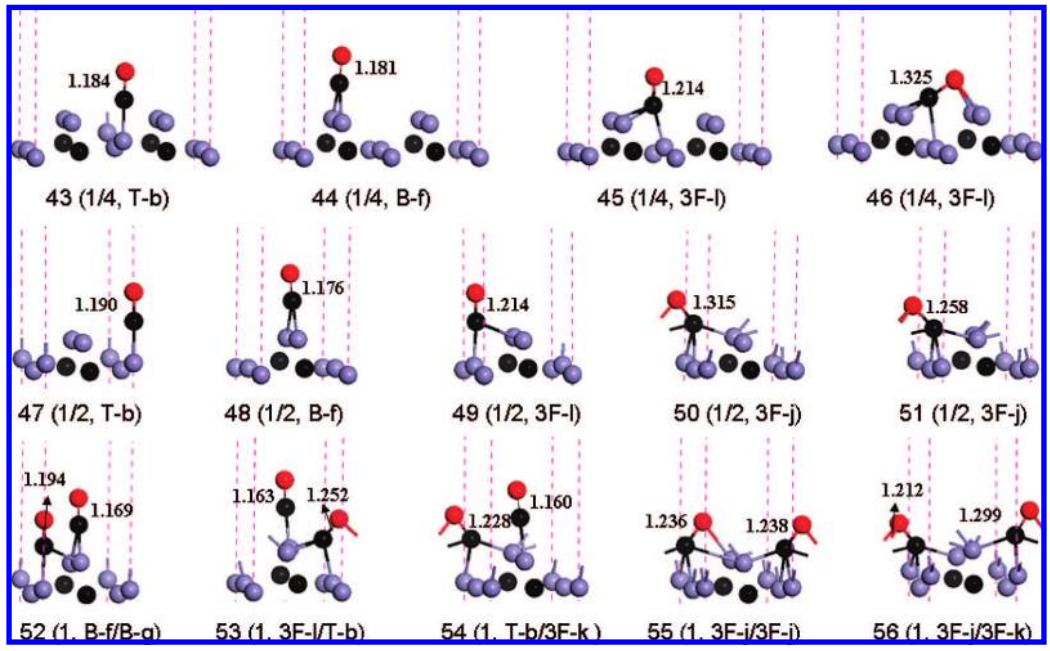

Figure 6. Side view of CO adsorption on (110) T_{Fe} (Fe, purple; C, black; O, red).

surface C. At 1/4 ML, **70** is the most stable adsorption configuration with CO on the C-top site.

At 1/2 ML, CO adsorbed sites can be considered as combinations of the occupied sites at 1/4 ML. As shown in Figure 8, structure **75** (T-c/3F-q) is similar to **77** (T-c/3F-q); the only difference is the transferred surface carbon in **77**. Furthermore, the adsorption energy of **77** (−1.74 eV) is more negative than that of **75** (−1.53 eV), indicating the repulsive interaction between CO and the surface in **75** is stronger than that in **77**.

(g) Surface Structure and Coverage. Table 8 shows that CO adsorption results in changes in the surface energy on the basis of the free optimized surface and that surface by deleting adsorbed CO molecules. For CO adsorption on iron atoms, the

TABLE 5: Calculated Adsorption Energies (E_{ads}, eV) per CO and Bond Lengths (d, Å) As Well As Net Charges (q, e) of CO on (110) T_{Fe} at 1/4, 1/2, and 1 ML

no.	θ	E_{ads}[a]	d_{C-O}	d_{Fe-C}	d_{O-Fe}	q_{CO}
43	1/4	−1.21 (−1.53)	1.184	1.745		−0.35
44	1/4	−2.04 (−2.29)	1.181	2.004, 1.886		−0.40
45	1/4	−1.61 (−1.99)	1.214	1.836, 2.078, 2.115		−0.59
46	1/4	−2.22 (−2.74)	1.325	2.081, 1.899, 1.912	2.027, 2.054	−0.81
47	1/2	−1.09 (−1.43)	1.190	1.752		−0.40
48	1/2	−1.93 (−2.20)	1.176	1.853, 2.124		−0.36
49	1/2	−1.52 (−1.92)	1.214	1.839, 2.247, 2.284		−0.64
50	1/2	−1.78 (−2.35)	1.315	1.947, 2.327, 1.875, 2.064	2.009, 2.073	−0.77
51	1/2	−1.72 (−2.21)	1.258	2.181, 2.207, 1.842, 2.068	1.996	−0.67
52	1	−1.41 (−1.77)	1.194	1.865, 2.110		−0.40
			1.169	1.813, 2.173		−0.28
53	1	−1.59 (−1.99)	1.163	1.777		−0.18
			1.252	1.927, 2.066, 1.881	2.068	−0.63
54	1	−1.38 (−1.77)	1.160	1.128		−0.17
			1.228	2.084, 1.846, 2.091		−0.54
55	1	−1.33 (−1.87)	1.236	2.226, 2.030, 1.866, 2.068	2.024	−0.56
			1.238	2.201, 2.031, 1.866, 2.061	2.021	−0.57
56	1	−1.18 (−1.69)	1.299	1.972, 2.069, 1.866, 2.030	1.958, 2.259	−0.72
			1.212	1.860, 1.964, 2.193	2.237	−0.45

[a] PBE values in parentheses.

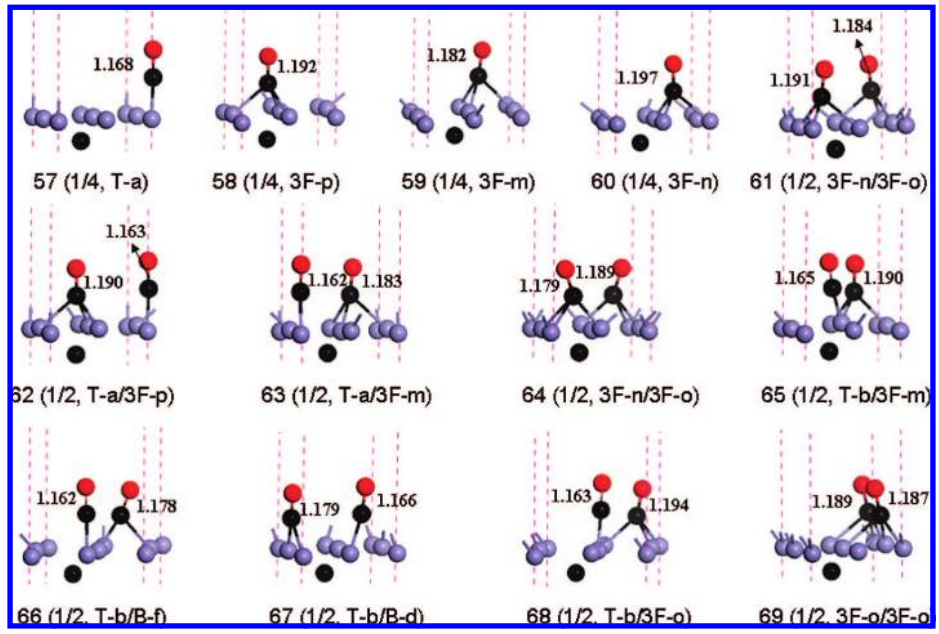

Figure 7. Side view of CO adsorption on (111) T_{Fe} (Fe, purple; C, black; O, red).

changes in the surface energy are relatively small (up to 3.55%), but CO adsorption on the surface carbon has a large change, up to 6.94%.

At this stage, it is interesting to compare the adsorption at all coverages. Along with a coverage increase, the adsorption energies of the most favored adsorption modes decrease (Table 9), and this is associated with the lateral interaction. Sung and Hoffmann[6] have carried out tight-binding calculations on hexagonal monolayer CO with nearest neighbor distances of 4.35, 3.29, and 2.51 Å. From the calculated band structure, they found that the interaction between two CO's at 4.35 Å is negligible, but is turned on at 3.29 Å, and the band widths attain several electron volts at 2.51 Å. In our calculations, the distances among the adsorbed CO are 5.28 Å at 1/4 ML. For (100) and (110), they decrease to 3.74 Å at 1/2 ML and to 2.63 and 2.48 Å at 1 ML, respectively. For (111), they decrease to 2.54 Å at 1/2 ML. As shown in Table 9, the changes of the adsorption energies are not obvious on (100) and (110) as the CO coverage increases from 1/4 to 1/2 ML. However, large decreases are found for (111) from 1/4 to 1/2 ML, and for (100) and (110) from 1/2 to 1 ML.

It is also interesting to note the formation of surface ketenylidene (C═C═O) species on (100) $T_{Fe/C}$, (100) $T_{Fe/C}$, and (111) T_C. Indeed, Kolis et al. confirmed the existence of the ketenylidene functionality by ^{13}C NMR spectroscopy and proposed the migration of a CO to the exposed carbide atom to form ketenylidene.[49] The existence of ketenylidene has been verified by a recent in situ IR study of CO adsorbed on fresh β-Mo_2C.[50]

On the basis of X-ray photoelectron spectroscopy, ketene (H_2C═C═O) could be formed on Fe by the following way: CO insertion into a surface carbon to form ketenylidene, followed by hydrogenation ($C_s + CO \rightarrow C$═C═O $\rightarrow H_2C$═C═O).[51] Our previous theoretical study on the adsorption of CO and H_2 on Fe_5C_2(001) and (110) showed the formation of surface ketenylidene from CO insertion into surface carbon and the

TABLE 6: Calculated Adsorption Energies (E_{ads}, eV) per CO and Bond Lengths (d, Å) As Well As Net Charges (e) of CO on (111) T_{Fe} at 1/4 and 1/2 ML

no.	θ	E_{ads}[a]	d_{C-O}	d_{Fe-C}	q_{CO}
57	1/4	−1.62 (−1.90)	1.168	1.782	−0.24
58	1/4	−1.34 (−1.68)	1.192	2.065, 2.062, 2.045	−0.46
59	1/4	−2.16 (−2.54)	1.182	2.293, 2.265, 1.793	−0.39
60	1/4	−1.65 (−2.04)	1.197	2.009, 1.992, 2.026	−0.49
61	1/2	−1.68 (−2.11)	1.184	1.814, 2.194, 2.194	−0.39
			1.191	1.829, 2.119, 2.121	−0.44
62	1/2	−1.20 (−1.56)	1.163	1.783	−0.16
			1.190	2.054, 2.039, 2.036	−0.41
63	1/2	−1.61 (−1.98)	1.162	1.782	−0.16
			1.183	2.203, 2.208, 1.804	−0.40
64	1/2	−1.81 (−2.21)	1.179	2.253, 2.255, 1.812	−0.35
			1.189	2.207, 2.077, 1.830	−0.43
65	1/2	−1.71 (−2.09)	1.165	1.781	−0.21
			1.190	2.041, 2.025	−0.46
66	1/2	−1.70 (−2.07)	1.162	1.763	−0.16
			1.178	2.257, 1.789	−0.35
67	1/2	−1.71 (−2.08).	1.166	1.768	−0.20
			1.179	2.228, 1.791	−0.36
68	1/2	−1.71 (−2.09)	1.163	1.764	−0.17
			1.194	2.037, 1.901, 2.054	−0.49
69	1/2	−1.64 (−2.08)	1.189	2.089, 1.835, 2.173	−0.43
			1.187	2.090, 1.837, 2.139	−0.43

[a] PBE values in parentheses.

TABLE 7: Calculated Adsorption Energies (E_{ads}, eV) per CO and Bond Lengths (d, Å) As Well As Net Charges (q, e) of CO on (111) T_C at 1/4 and 1/2 ML

no.	θ	E_{ads}[a]	d_{C-O}	d_{C-C}	d_{Fe-C}	d_{Fe-O}	q_{CO}
70	1/4	−2.08 (−2.19)	1.175	1.302			0.01
71	1/4	−0.94 (−1.27)	1.162		1.799		−0.16
72	1/4	−1.53 (−1.86)	1.243	1.328	2.182, 2.207, 2.196	2.199	−0.47
73	1/4	−1.87 (−2.32)	1.191		1.980, 1.999, 1.967		−0.45
74	1/2	−1.50 (−1.76)	1.172	1.301			0.06
			1.166		1.778		−0.19
75	1/2	−1.53 (−1.86)	1.166	1.313	0.12		
			1.200		2.182, 1.925, 1.931		−0.47
76	1/2	−1.38 (−1.71)	1.164	1.320			0.14
			1.262	1.450	2.038, 2.000, 1.997	2.174	−0.61
77	1/2	−1.74 (−2.06)	1.164	1.316			0.12
			1.189		2.232, 1.805, 2.284		−0.41

[a] PBE values in parentheses.

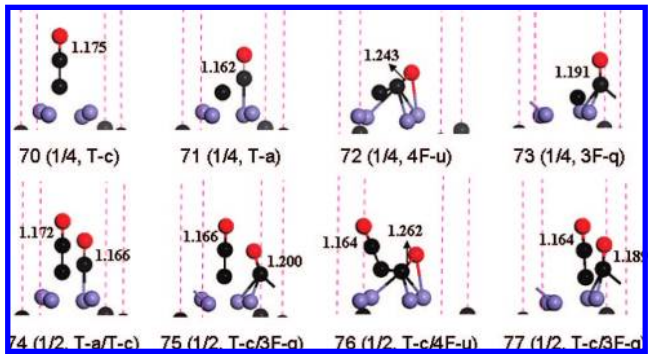

Figure 8. Side view of CO adsorption on (111) T_C (Fe, purple; C, black; O, red).

formation of surface ketene by ketenylidene hydrogenation.[31,32,52] For CO adsorption on α-Mo_2C(0001)[53] and on the lower index surfaces of Fe_3C,[30] a similar phenomenon has been found. Ketene has been considered as a principal intermediate for C_2 hydrocarbons and oxygenates in FTS. Hence, we conclude that the surface ketenylidene (C═C═O) species may be the precursor of CO activation and dissociation.

DFT calculations have shown that the CO dissociation pathway is highly associated with the properties and structures of the metals. Liu and Hu found that surface defects, such as steps and kinks, can largely facilitate bond breaking. For CO ↔ C + O reaction, the dissociation barriers are reduced larger than 0.8 eV by steps and kinks of Rh and Pd.[54] The work of Ciobica and van Santen suggested that the direct CO dissociation path is favorable over stepped Ru(0001), but not preferred on Pd(111) and flat Ru(0001).[55] Recently, a comprehensive work of ultrahigh-vacuum experiments and DFT calculations by Nørskov et al. revealed that under methanation conditions, CO dissociation proceeds most favorably on low-coordinated sites of nickel surfaces with COH as intermediate.[56] Furthermore,

TABLE 8: Changes in the Surface Energy (RPBE, J/m^2) upon CO Adsorption

surface	E_{surf}[a]	$E_{surf,re}$[b]	ΔE
(100) T_{Fe}	2.14	2.15	0.01 (0.47%)
(100) $T_{Fe/C}$	1.97	2.04	0.07 (3.55%)
(110) $T_{Fe/C}$	2.47	2.48	0.01 (0.40%)
(110) T_{Fe}	2.51	2.54	0.03 (1.20%)
(111) T_{Fe}	2.48	2.51	0.03 (1.21%)
(111) T_C	2.45	2.62	0.17 (6.94%)

[a] Energy of free optimized surface. [b] Energy of reconstructed surface by CO adsorption (by removal of the adsorbed CO).

TABLE 9: The Change of Adsorption Energy for the Most Stable Adsorption Configurations upon Coverage Increase

surfaces	ΔE_{ads} (eV) 1/4 ML → 1/2 ML	ΔE_{ads} (eV) 1/2 ML → 1 ML
(100) T_{Fe}	0.09 (4.55%) (**3** → **7**)	0.84 (44.44%) (**7** → **8**)
(100) $T_{Fe/C}$	0.02 (1.82%) (**15** → **17**)	0.24 (22.22%) (**17** → **20**)
(110) $T_{Fe/C}$	−0.05 (−3.29%) (**26** → **32**)	0.37 (23.57%) (**32** → **38**)
(110) T_{Fe}	0.29 (13.06%) (**46** → **48**)	0.34 (17.62%) (**48** → **53**)
(111) T_{Fe}	0.35 (16.20%) (**59** → **62**)	
(111) T_C	0.34 (16.35%) (**70** → **77**)	

some detailed DFT studies supported that the CHO species is likely an important intermediate ($CO_{ads} + H_{ads} \rightarrow CHO_{ads}$; $CHO_{ads} \rightarrow CH_{ads} + O_{ads}$) in FTS, especially for Fe- and Co-based catalytic processes.[28,57−59]

Moreover, surface C−C bonds are important for the exchange of carbon, and surface C−C coupling in FTS has been verified by Stockwell et al. with ^{13}C traces,[60] and they found that surface carbon atoms of carbide catalysts are incorporated into the FTS products. All these indicate that the participation of surface C sites plays an essential role in many reactions on metal carbide surfaces. Therefore, detailed understanding of the reaction mechanisms is the driving force of our study.

(h) Electronic Properties. A vast amount of literature has discussed the nature of the interaction between CO and transition metals. It has been shown that the donation and back-donation between the frontier orbitals of adsorbed CO and the surface metal are essential for CO activation; that is, the HOMO electrons of adsorbed CO donate to the LUMO of surface metal atoms, whereas in turn, the d electrons of surface metal atoms donate back to the LUMO of adsorbed CO, resulting in weakening and elongation of the strong C≡O bond, and CO is therefore activated.[61,62]

To understand the CO binding mechanism on Fe_4C, the PDOS of the adsorbed CO was analyzed. The PDOS were obtained by projecting onto the molecular orbitals of CO, which are the sum of the C and O atoms. Figure 9 gives the PDOS of CO in the most stable adsorbed states **3**, **15**, **26**, **46**, **59**, and **70** at 1/4 ML, and **7**, **17**, **32**, and **48** at 1/2 ML. As shown in Figure 9, the 5σ orbital of free CO is at the Fermi level, and the $2\pi^*$ is at about 7 eV. Configurations **3** and **7** are the most stable adsorption structures on (100) T_{Fe} at 1/4 and 1/2 ML, respectively. Both the adsorption energies (−1.98 and −1.89 eV) and the structures (4F-r) are similar. The 5σ orbital of adsorbed CO shifts downward to −6.70 and −6.57 eV, and the $2\pi^*$ orbitals shift downward to −2.33 and −2.65 eV, respectively. The shifts of 5σ and $2\pi^*$ are primary results of 5σ donation and $2\pi^*$ back-donation. The partial electron transfer leads to the $2\pi^*$ band below the Fermi level, and the significant elongation of the C−O bond is due to the antibonding nature of the $2\pi^*$ orbitals. In **15**, the 5σ orbital of the adsorbed CO shifts downward to −6.57 eV, and the $2\pi^*$ orbital shifts downward to −1.43 eV. In **17**, the 5σ and $2\pi^*$ orbitals of the adsorbed CO shift downward to −6.55 and 3.45 eV, respectively. When compared to the PDOS of **17**, the $2\pi^*$ orbital of the adsorbed CO in **15** shifts downward more; this is because more electrons transfer from the surface to **15** (0.57 e) than to **17** (0.15 e).

Configurations **26** and **32** are the most stable adsorption configurations on (110) $T_{Fe/C}$ at 1/4 and 1/2 ML, respectively, and they have close adsorption energies (−1.52 and −1.57 eV) and similar structures (Fe_2-top). The 5σ orbital of the adsorbed CO shifts downward to −6.30 and −6.18 eV, and the $2\pi^*$ orbitals shift downward to 3.47 and 3.71 eV, respectively. The $2\pi^*$ orbitals of the adsorbed CO in **46** shift downward to −2.46 eV, quite below the Fermi level, indicating a very large charge transfer to CO (−0.59 e). In **59**, the 5σ and $2\pi^*$ orbitals of the

TABLE 10: Comparison of the Largest Energies for CO Adsorbed on Fe, Fe_4C, Fe_3C and Fe_5C_2 at Low Coverage

surface	method	θ	site	E_{ads} (eV)	d_{C-O} (Å)	q_{CO}	ref
Fe							
(100)	RPBE	1/4	4-fold	−1.49	1.321		15
	PBE		4-fold	−2.08	1.321		
	Exp.			−1.11			64
(110)	RPBE	1/4	on-top	−1.58			14
	PBE		on-top	−1.88			
	exp			−1.24			65
(111)	RPBE	1/3	Shallow-hollow	−2.08	1.191	−0.46	28
	PBE		Shallow-hollow	−2.45	1.191		26
Fe_4C							*a*
(100) T_{Fe}	RPBE	1/4	4-fold	−1.98	1.288	−0.80	
	PBE			−2.53			
(100) $T_{Fe/C}$	RPBE	1/4	4-fold	−1.10	1.211	−0.57	
	PBE			−1.54			
(110) $T_{Fe/C}$	RPBE	1/4	on-top	−1.52	1.166	−0.21	
	PBE			−1.81			
(110) T_{Fe}	RPBE	1/4	3-fold	−2.22	1.325	−0.81	
	PBE			−2.74			
(111) T_{Fe}	RPBE	1/4	3-fold	−2.16	1.182	−0.39	
	PBE			−2.54			
(111) T_C	RPBE	1/4	on-top	−2.08	1.175	0.01	
	PBE			−2.19			
Fe_3C							30
(100)	RPBE	1/5	3-fold	−1.77	1.204	−0.57	
(001)	RPBE	1/6	4-fold	−1.79	1.209	−0.57	
(010)	RPBE	1/3	2-fold	−2.03	1.174	−0.32	
Fe_5C_2							31
(100)	PBE	1/4	3-fold	−2.21	1.200		
(001)	PBE	1/6	3-fold	−2.10	1.259		
(110)	PBE	1/6	3-fold	−2.34	1.199		

[a] This work.

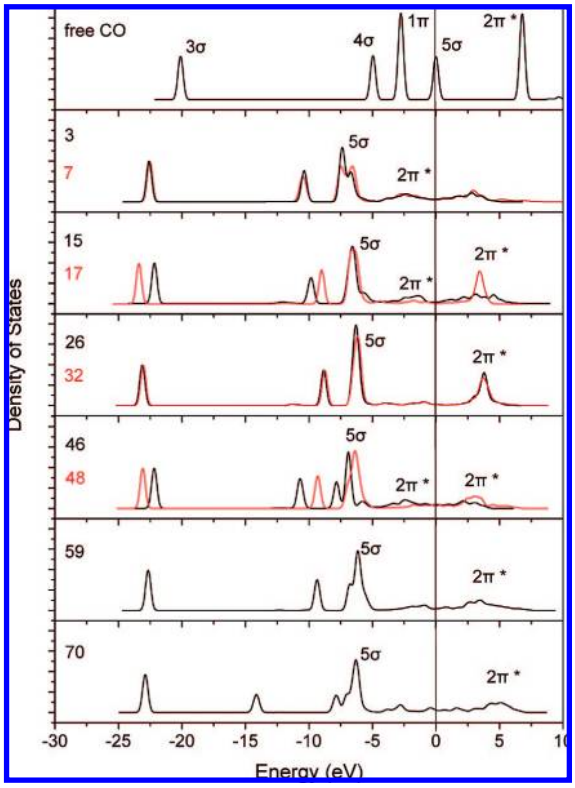

Figure 9. Partial density of states of free and the adsorbed CO of the most stable configurations at low coverage on (100), (110), and (111).

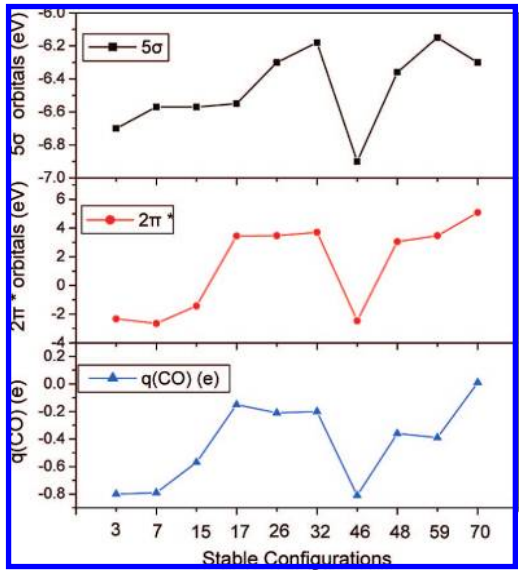

Figure 10. The 5σ and $2\pi^*$ orbitals and the net charge (q) of the adsorbed CO of the stable configurations.

adsorbed CO shift downward to −6.15 and 3.47 eV, respectively. The 5σ band of the adsorbed CO in **70** shifts downward to −6.30 eV, and the $2\pi^*$ band shifts downward to 5.08 eV.

On the basis of the above results, we found that the shift of 5σ and $2\pi^*$ orbitals of the adsorbed CO has a trend that is similar to the electron transfer from the surface to the adsorbed CO, as shown in Figure 10; that is, the more the electron transfer, the more the downward shift of 5σ and $2\pi^*$ orbitals.

(i) Factor Controlling C−O Bond Activation. From the point of view of catalysis, it is important to find out the factors controlling the activation degree of CO on the Fe_4C surfaces.

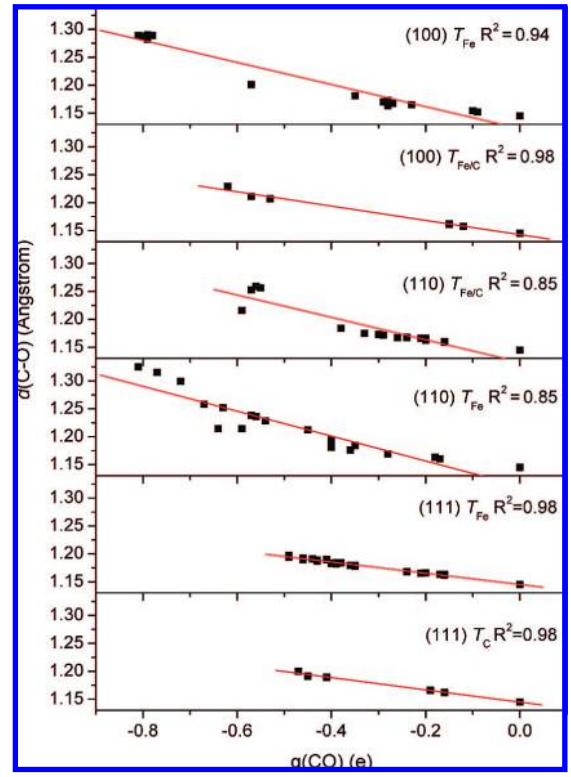

Figure 11. Linear relationship of the net charge (q) and the C−O bond lengths of CO on (100), (110), and (111).

The net charges of the adsorbed CO on the Fe_4C surface are given in Tables 2−7. When compared with those of free CO, the adsorbed CO molecules are partially negatively charged, indicating electron transfer from the Fe_4C surface to CO. As shown in Figure 11, the elongation of the C−O bonds increases with the increases in the net negative charges of the adsorbed CO molecules. It indicates that the C−O bond lengths (d) of the adsorbed CO have a linear relationship with their net charges (q) (R^2 = 0.94, 0.98, 0.85, and 0.98 for (100) T_{Fe}, (100) $T_{Fe/C}$, (110), and (111), respectively). Wang et al. have found similar results in CO_2 chemisorption on transition metal surfaces;[63] that is, the activation degree of C═O bonds in CO_2 has a linear relationship with the transferred charges from the metal surfaces. However, no correlation between the binding energy and net charge of CO can be found.

For the (100) and (110) surfaces, compared to $T_{Fe/C}$, T_{Fe} can transfer more electrons and have a larger slope coefficient of the fitted linear regression line, and this reveals that T_{Fe} can activate CO more strongly than $T_{Fe/C}$. It is noteworthy that the formation of the Fe−O bond on the (100) T_{Fe}, (110) $T_{Fe/C}$, and T_{Fe} surfaces leads to stronger electron transfer from surface iron atoms to adsorbed CO. For (111), CO mainly adsorbs uprightly at the multicoordination sites on the T_{Fe} surface that has a closely packed structure, and the net charges are less than that of the titled adsorption configurations with the formation of Fe−O bond. The T_C has a very open surface, and CO could also bond to the Fe atoms of the second layer; therefore, it has properties similar to those of the T_{Fe}. In summary, the activation degree of C−O bonds in CO has a linear relationship with the charges received. Therefore, we could modify its activation degree by improving the surface ability of the presenting electrons.

(j) Comparison with Fe, Fe_3C, and Fe_5C_2. On the basis of the adsorption data, it is interesting to compare the most stable CO adsorption on Fe_4C with those on different Fe, Fe_3C, and Fe_5C_2 surfaces (Table 10). It shows clearly that the configura-

tions with CO adsorbed on pure iron termination surfaces of iron carbides tend to have larger adsorption energies than those on low-indexed surfaces of iron, indicating that the formation of iron carbides is advantageous for the CO adsorption. It also confirms that iron carbides are FTS active phases from another perspective.

It should be noted that the surfaces of Fe_4C, Fe_3C, and Fe_5C_2 with only iron atoms have stronger CO adsorption energies as compared with those containing both surface iron and carbon atoms (-2.22 vs -1.52, -2.03 vs -1.77, -2.34 vs -2.10). On the basis of the adsorption energy data, it is found that CO prefers to adsorb at multicoordination sites. We also found that the adsorbed CO of the most stable adsorption configuration on most of the surfaces bonds to the surface iron atoms, indicating that CO prefers to adsorb around iron atoms.

4. Conclusion

To explore the mechanism of FTS, CO adsorption on the low-indexed (100), (110), and (111) termination surfaces of Fe_4C at different coverage has been investigated at the level of density functional theory (PBE-GGA).

On the (100) T_{Fe} surface, the configurations with CO adsorbed at the 4-fold site ($2Fe_1-2Fe_2$) with the formation of Fe−O bond are most stable at both 1/4 and 1/2 ML coverage. With increased CO coverage, the repulsive interaction of the adsorbed CO molecules increases. At 1 ML coverage, the configuration with CO bridging over two Fe atoms (Fe_1-Fe_2) is most stable. On (100) $T_{Fe/C}$, the most stable adsorption site is the 4-fold site ($4Fe_2$) at 1/4 ML, whereas the Fe_2-top site is the most favored at 1/2 ML coverage. At 1 ML coverage, some adsorption configurations have positive adsorption energies, indicating that CO adsorption on (100) $T_{Fe/C}$ at high coverage is thermodynamically not favored.

On the (110) $T_{Fe/C}$ surface, the configurations with CO adsorbed at the Fe_2-top site are the most stable at both 1/4 and 1/2 ML coverage, whereas the C−O bond of CO is more activated at the 4-fold site ($Fe_1-Fe_2-Fe_2'-C$). At 1 ML coverage, the adsorption energy becomes lower because of the crowded distribution of surface species. The adsorption structure with one CO on a top site (Fe_1-top) and one on a 2-fold site (Fe_1-Fe_2) is the most stable. The pure iron termination surface of (110) has a steplike surface with atoms of the first and second layers exposed. At 1/4 ML coverage, the adsorption configuration with CO at the 3-fold site with the O atom bonding to two Fe atoms is the most stable. At 1/2 ML coverage, the most stable adsorption configuration has CO bridging Fe_2-Fe_2. At 1 ML, the adsorption configuration with one CO on the Fe_2-top site, and the other one at the 3-fold site ($Fe_1'-2Fe_2$) is the most stable.

The (111) T_{Fe} has a closely packed surface, and CO favors adsorption on the 3-fold sites at both 1/4 and 1/2 ML. In contrast, the (111) T_C has a very open structure surface, and the adsorption configuration with CO bonding on the C-top site is the most stable. From 1/4 to 1/2 ML, it is interesting to note the formation of the O−C−C−C−O geometric structure. It is also interesting to note the formation of surface ketenylidene (C═C═O) species on (100) $T_{Fe/C}$, (110) $T_{Fe/C}$, and (111) T_C, which may be the precursor for CO dissociation.

The bonding mechanism of CO to the surface is also analyzed by the help of PDOS. When compared with the 5σ and $2\pi^*$ orbitals of free CO, the 5σ orbital of the adsorbed CO shifts strongly downward, and part of the $2\pi^*$ orbitals of the adsorbed CO lies quite below the Fermi level. This indicates a charge transfer from the surface to CO. As a consequence, the adsorbed CO is partially negatively charged and has elongated C−O bond lengths. This is due to the enhanced electron transfer from the Fe_4C surface iron atoms to the CO, and the more the electron transfer, the stronger the CO activation.

Comparing the most stable CO adsorption configurations on Fe_4C with those on different Fe, Fe_3C, and Fe_5C_2 surfaces, we found that the formation of iron carbides is advantageous for the CO adsorption. It is also found that CO tends to favor adsorption sites with higher coordination and prefers to adsorb around iron atoms.

Acknowledgment. We thank the National Natural Science Foundation of China (No. 20873173) for financial support; and the National Outstanding Young Scientists Foundation of China (No. 20625620).

Supporting Information Available: This material is available free of charge via the Internet at http://pubs.acs.org.

References and Notes

(1) Eastman, D. E. *Solid State Commun.* **1972**, *10*, 933.
(2) Brodén, G.; Gafner, G.; Bonzel, H. *Appl. Phys.* **1977**, *13*, 33.
(3) Jensen, E. S.; Rhodin, T. N. *Phys. Rev. B* **1983**, *27*, 3338.
(4) Greuter, F.; Heskett, D.; Plummer, E. W.; Freund, H. J. *Phys. Rev. B* **1983**, *27*, 7117.
(5) Engel, T.; Ertl, G. *Adv. Catal.* **1979**, *28*, 1.
(6) Sung, S.-S.; Hoffmann, R. *J. Am. Chem. Soc.* **1985**, *107*, 578.
(7) Moon, D. W.; Dwyer, D. J.; Bernasek, S. L. *Surf. Sci.* **1985**, *163*, 215.
(8) Seip, U.; Tsai, M. C.; Christmann, K.; Kuppers, J.; Ertl, G. *Surf. Sci.* **1984**, *139*, 29.
(9) Bartosch, C. E.; Whitman, L. J.; Ho, W. *J. Chem. Phys.* **1986**, *85*, 1052.
(10) Lemire, C.; Meyer, R.; Henrich, V. E.; Shaikhutdinov, Sh.; Freund, H. J. *Surf. Sci.* **2004**, *572*, 103.
(11) Sorescu, D.; Thompson, D. L.; Hurley, M. M.; Chabalowski, C. F. *Phys. Rev. B* **2002**, *66*, 035416.
(12) Nayak, S. K.; Nooijen, M.; Bernasek, S. L.; Blaha, P. *J. Phys. Chem. B* **2001**, *105*, 164.
(13) Stibor, A.; Kresse, G.; Eichler, A.; Hafner, J. *Surf. Sci.* **2002**, *507−510*, 99.
(14) Jiang, D. E.; Carter, E. A. *Surf. Sci.* **2004**, *570*, 167.
(15) Jiang, D. E.; Carter, E. A. *J. Phys. Chem. B* **2006**, *110*, 22213.
(16) Sirimanothan, N.; Hamdeh, H. H.; Zhang, Y.; Davis, B. H. *Catal. Lett.* **2002**, *82*, 181.
(17) Dwyer, D. J.; Somorjai, G. A. *J. Catal.* **1978**, *52*, 291.
(18) Reymond, J. P.; Meriaudeau, P.; Teichner, S. J. *J. Catal.* **1982**, *75*, 39.
(19) Kuivila, C. S.; Stair, P. C.; Butt, J. B. *J. Catal.* **1989**, *118*, 299.
(20) Le Caër, G.; Dubois, J. M.; Pijolat, M.; Perrichon, V.; Bussière, P. *J. Phys. Chem.* **1982**, *86*, 4799.
(21) Shultz, J. F.; Hall, W. K.; Dubs, T. A.; Anderson, R. B. *J. Am. Chem. Soc.* **1956**, *78*, 282.
(22) Rao, K. R. P. M.; Huggins, F. E.; Mahajan, V.; Huffman, G. P.; Rao, V. U. S.; Bhatt, B. L.; Bukur, D. B.; Davis, B. H.; O'Brien, R. J. *Top. Catal.* **1995**, *2*, 71.
(23) Mansker, L. D.; Jin, Y.; Burker, D. B.; Datye, A. K. *Appl. Catal., A* **1999**, *186*, 277.
(24) Dictor, R.; Bell, A. T. *J. Catal.* **1986**, *97*, 121.
(25) Amelse, J. A.; Butt, J. B.; Schwartz, L. H. *J. Phys. Chem.* **1978**, *82*, 558.
(26) Chen, Y.-H.; Cao, D.-B.; Yang, J.; Li, Y.-W.; Wang, J.; Jiao, H. *Chem. Phys. Lett.* **2004**, *400*, 35.
(27) Ma, Z.-Y.; Huo, C.-F.; Liao, X.-Y.; Li, Y.-W.; Wang, J.; Jiao, H. *J. Phys. Chem. C* **2007**, *111*, 4305.
(28) Huo, C.-F.; Ren, J.; Li, Y.-W.; Wang, J.; Jiao, H. *J. Catal.* **2007**, *249*, 174.
(29) Huang, D.-M.; Cao, D.-B.; Li, Y.-W.; Jiao, H. *J. Phys. Chem. B* **2006**, *110*, 13920.
(30) (a) Liao, X.-Y.; Cao, D.-B.; Wang, S.-G.; Ma, Z.-Y.; Li, Y.-W.; Wang, J.; Jiao, H. *J. Mol. Catal. A: Chem.* **2007**, *269*, 169. (b) Liao, X.-Y.; Wang, S.-G.; Ma, Z.-Y.; Li, Y.-W.; Wang, J. G.; Jiao, H. *J. Mol. Catal. A: Chem.* **2008**, *292*, 14.
(31) Cao, D.-B.; Zhang, F.-Q.; Li, Y.-W.; Jiao, H. *J. Phys. Chem. B* **2004**, *108*, 9094.
(32) Cao, D.-B.; Zhang, F.-Q.; Li, Y.-W.; Jiao, H. *J. Phys. Chem. B* **2005**, *109*, 10922.

(33) Shevchenko, E. V.; Talapin, D. V.; Murray, C. B.; O'Brien, S. *J. Am. Chem. Soc.* **2006**, *128*, 3620.
(34) Choo, W. K.; Kaplow, R. *Acta Metall.* **1973**, *21*, 725.
(35) Deng, C.-M.; Huo, C.-F.; Bao, L.-L.; Shi, X.-R.; Li, Y.-W.; Wang, J.; Jiao, H. *Chem. Phys. Lett.* **2007**, *448*, 83.
(36) Santos, A. V.; Costa, M. I.; Kuhnen, C. A. *J. Magn. Magn. Mater.* **1997**, *166*, 223.
(37) Hohenberg, P.; Kohn, W. *Phys. Rev.* **1964**, *136*, B864.
(38) Kohn, W.; Sham, L. J. *Phys. Rev.* **1965**, *140*, A1133.
(39) Payne, M. C.; Teter, M. P.; Allan, D. C.; Arias, T. A.; Joannopoulos, J. D. *Rev. Mod. Phys.* **1992**, *64*, 1045.
(40) Milman, V.; Winkler, B.; White, J. A.; Pickard, C. J.; Payne, M. C.; Akhmataskaya, E. V.; Nobes, R. H. *Int. J. Quantum Chem.* **2000**, *77*, 895.
(41) Segall, M. D.; Lindan, P. J. D.; Probert, M. J.; Pickard, C. J.; Hasnip, P. J.; Clark, S. J.; Payne, M. C. *J. Phys.: Condens. Matter* **2002**, *14*, 2717.
(42) Perdew, J. P.; Burke, S.; Ernzerhof, M. *Phys. Rev. Lett.* **1996**, *77*, 3865.
(43) White, J. A.; Bird, D. M. *Phys. Rev. B* **1994**, *50*, 4954.
(44) Vanderbilt, D. *Phys. Rev. B* **1990**, *41*, 7892.
(45) Monkhorst, H. J.; Pack, J. D. *Phys. Rev. B* **1976**, *13*, 5188.
(46) Hammer, B.; Hansen, L. B.; Nørskov, J. K. *Phys. Rev. B* **1999**, *59*, 7413.
(47) Zhang, Y.; Yang, W. *Phys. Rev. Lett.* **1998**, *80*, 890.
(48) Peltzer y Biancá, E. L.; Desimoni, J.; Christensen, N. E. *Phys. B* **2004**, *354*, 341.
(49) Kolis, J. W.; Holt, E. M.; Shriver, D. F. *J. Am. Chem. Soc.* **1983**, *105*, 7307.
(50) Wu, W.; Wu, Z.; Liang, C.; Chen, X.; Ying, P.; Li, C. *J. Phys. Chem. B* **2003**, *107*, 7088.
(51) Loggenberg, P. M.; Carlton, L.; Copperthwaite, R. G.; Hutchings, G. J. *J. Chem. Soc., Chem. Commun.* **1987**, 541.
(52) (a) Cao, D.-B.; Wang, S.-G.; Li, Y.-W.; Wang, J.; Jiao, H. *J. Mol. Catal. A: Chem.* **2007**, *272*, 275. (b) Cao, D.-B.; Li, Y.-W.; Wang, J.; Jiao, H. *J. Phys. Chem. C* **2008**, *112*, 14884.
(53) Ren, J.; Huo, C.-F.; Wang, J.; Li, Y.-W.; Jiao, H. *Surf. Sci.* **2005**, *596*, 212.
(54) Liu, Z.-P.; Hu, P. *J. Am. Chem. Soc.* **2003**, *125*, 1958.
(55) Ciobica, I. M.; van Santen, R. A. *J. Phys. Chem. B* **2003**, *107*, 3808.
(56) Andersson, M. P.; Abild-Pedersen, F.; Remediakis, I.; Bligaard, T.; Jones, G.; Engbæk, J.; Lytken, O.; Horch, S.; Nielsen, J. H.; Sehested, J.; Rostrup-Nielsen, J. R.; Nørskov, J. K.; Chorkendorff, I. *J. Catal.* **2008**, *255*, 6.
(57) Inderwildi, O. R.; Jenkins, S. J.; King, D. A. *J. Phys. Chem. C* **2008**, *112*, 1305.
(58) Inderwildi, O. R.; Jenkins, S. J.; King, D. A. *Angew. Chem., Int. Ed.* **2008**, *47*, 1.
(59) Huo, C.-F.; Li, Y.-W.; Wang, J.; Jiao, H. *J. Phys. Chem. C* **2008**, *112*, 14108.
(60) Stockwell, D. M.; Bianchi, D.; Bennett, C. O. *J. Catal.* **1988**, *113*, 13.
(61) Blyholder, G. *J. Phys. Chem.* **1964**, *68*, 2772.
(62) Pavão, A. C.; Guimarães, T. C. F.; Lie, S. K.; Taft, C. A.; Lester, W. A., Jr *J. Mol. Struct.* **1999**, *458*, 99.
(63) Wang, S.-G.; Liao, X.-Y.; Cao, D.-B.; Huo, C.-F.; Li, Y.-W.; Wang, J.; Jiao, H. *J. Phys. Chem. C* **2007**, *111*, 16934.
(64) Moon, D. W.; Dwyer, D. J.; Bernasek, S. L. *Surf. Sci.* **1985**, *163*, 215.
(65) Wedler, G.; Ruhmann, R. *Appl. Surf. Sci.* **1983**, *14*, 137.

JP805702N